Supporting Information

Surfactant-mediated preparation of fully waterborne robust superamphiphobic coatings for anti-icing

Yongtao Ren,[a] Bucheng Li,*[a] and Junping Zhang*[ab]

[a] Research Center of Resource Chemistry and Energy Materials, Lanzhou Institute of Chemical Physics, Chinese Academy of Sciences, Lanzhou, Gansu 730000, China

[b] Center of Materials Science and Optoelectronics Engineering, University of Chinese Academy of Sciences, Beijing 100049, China

*Corresponding authors: libucheng111@163.com, jpzhang@licp.cas.cn

Materials

SiO_2 nanoparticles (10-20 nm) were obtained from Maikun Chemical Co., Ltd. Tetraethoxysilane (99.9%) and perfluorodecyltriethoxysilane (97%) were obtained from Gelest. (Shanghai, China). Surfactants FS-61, Zonyl 321, and FS-3100 were obtained from (J&K Scientific), (Dongguan Yingsheng Plastic & Chemical Co., Ltd), and (Tianjin Fuyu Fine Chemical Co., Ltd), respectively. The waterborne polyurethane was supplied by Shandong Xinna Superhydrophobic New Materials Co., Ltd. (China). Glass slides were obtained from Citotest Scientific Co., Ltd. (China). Aluminum alloy, copper alloy, magnesium alloy and stainless steel plates were sourced from Shanghai Haocheng Metal Material Co., Ltd. (China).

Droplets impact test

The dynamic impact behavior of liquid droplets was investigated by releasing 10 μL droplets from a 1 cm or 1 m height onto the coating surface, with the entire impact process captured using high-speed videography (FASTCAM Mini UX100) at a temporal resolution of 4,000 fps.

Mechanical, chemical, and environmental durability tests

Mechanical performance of the coatings was characterized using Taber abrasion testing (CS-10 wheel, 125g load, ASTM D4060) and tape peel adhesion testing (3M Scotch 600, 0.2 kg load, ASTM D3359).

For the water jet impact test, the coatings were fixed on a 45° inclined platform and subjected to impact by a stable water jet (nozzle diameter 1.8 mm, flow velocity 4.3 m/s), with the jet exit positioned 20 cm away from the sample. After each impact test, the sample surface was dried with a hot air blower, followed by immediate measurement of the water CA and SA.

Chemical resistance was assessed by immersing the same set of samples in 0.1 M HCl aqueous solution, 0.1 M NaCl aqueous solution and various organic solvents, with periodic wettability measurements to track performance changes.

The UV aging resistance of the coatings were evaluated using a WFH-204B UV lamp with a primary wavelength of 365 nm and a power output of 12 W. The coated samples were placed horizontally at a fixed distance of 5 cm from the lamp outlet.

Outdoor durability assessment was conducted by exposing the coated samples on an acrylic panel in Lanzhou, China, from March 16 to April 15, 2024, to evaluate the stability under real-world late winter to early spring conditions. Throughout the entire exposure period, the same set of samples was monitored at each interval to track performance evolution. The samples were mounted at a 45° tilt angle facing south to maximize solar exposure and simulate service conditions of an inclined surface.

Throughout all durability evaluations, CA and SA measurements were conducted at predetermined intervals to quantitatively monitor coating degradation.

Anti-icing performance tests

A 60 μL water droplet was deposited on the samples in a controlled environment (-10 °C, 60% RH) using a custom refrigeration setup. The time required for complete freezing was determined by continuous monitoring with a CCD camera.

Ice adhesion strength was quantified by freezing a 1.0 mL water droplet in a glass cylinder placed on the coating surface for 2 h. The tensile force required to detach the ice column was measured using a digital force gauge, with the adhesion strength (τ, kPa) calculated as the ratio of the measured force (F, N) to the contact area (A, m^2) between the ice and substrate.

Characterization

The wettability of the samples was evaluated using an OCA20 contact angle system (Dataphysics, Germany), with droplets (10 μL) for both CA and SA measurements (n=5). High-speed droplet impact dynamics were captured at 4000 fps (FASTCAM Mini UX100). Surface morphology was characterized by field emission SEM (JSM-6701F, JEOL) and TEM (JEM-1200EX, JEOL). Elemental mapping of samples was determined by energy-dispersive X-ray spectroscopy (EDS) using an Oxford Instruments X-Max 80 silicon drift detector (SDD)

attached to the FE-SEM. Chemical composition analysis included XPS (ESCALAB 250Xi, Al Kα radiation) and FTIR spectroscopy (Thermo Nicolet NEXUS TM, 4000-400 cm^{-1}, KBr pellets). The surface topography was quantified using a Bruker Contour GT-K Optical Profiler equipped with a 50X objective lens and operating in Vertical Scanning Interferometry (VSI) mode. The measurements were performed over a scan area of 227.8 μm × 170.9 μm. The surface free energy of the coatings was determined using the Owens-Wendt-Rabel-Kaelble (OWRK) method. Static contact angles of two probe liquids with known polar and dispersive components, deionized water (polar liquid) and diiodomethane (dispersive liquid) were measured on the coated surfaces using a OCA20 contact angle system. For each sample, at least five measurements were taken at different locations on the surface with a droplet volume of 5 μL. The average values of these contact angles were then used to calculate the total surface free energy components via the OWRK model integrated into the instrument's software (OCA20).

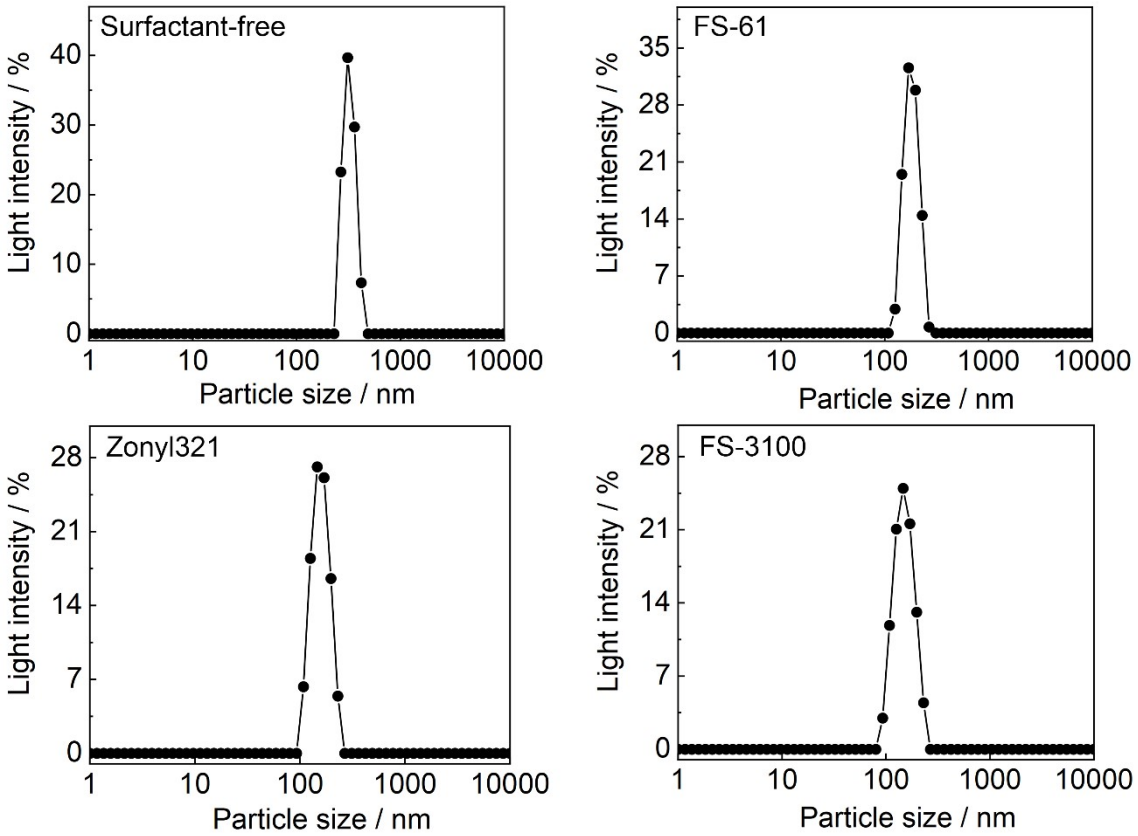

Fig. S1. Particle size distribution of F-POS@SiO_2 prepared with different surfactants.

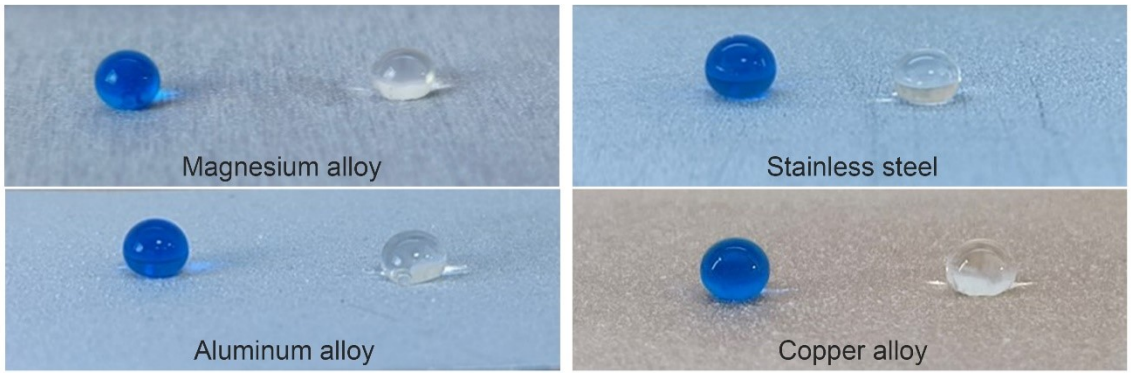

Fig. S2. Water and oil droplets on the WPU/F-POS@SiO_2 coatings on different substrates.

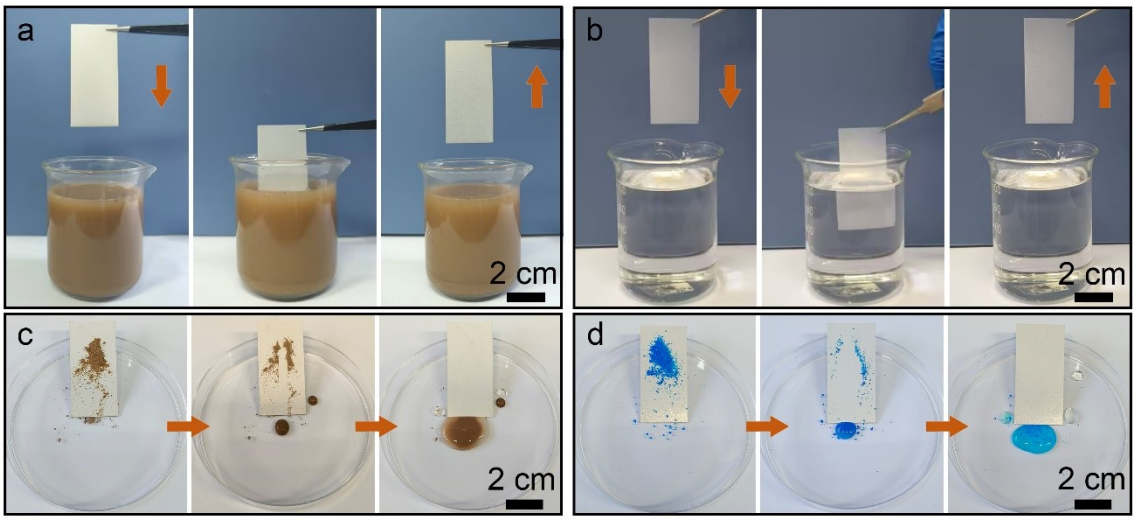

Fig. S3. Anti-fouling test of the coating in (a) muddy water and (b) *n*-hexadecane. Self-cleaning behavior of the coating against (c) dust and (d) $Cu(NO_3)_2$ powder.

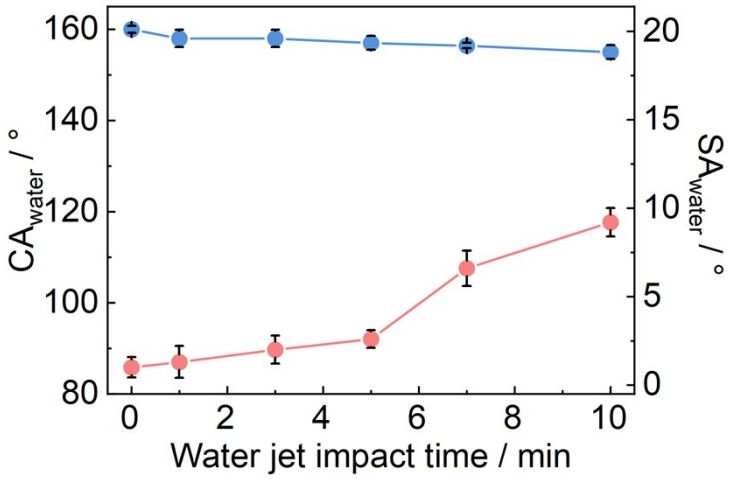

Fig. S4. Variations of CA_{water} and SA_{water} on the WPU/F-POS@SiO_2 coating during the water jet impact test.

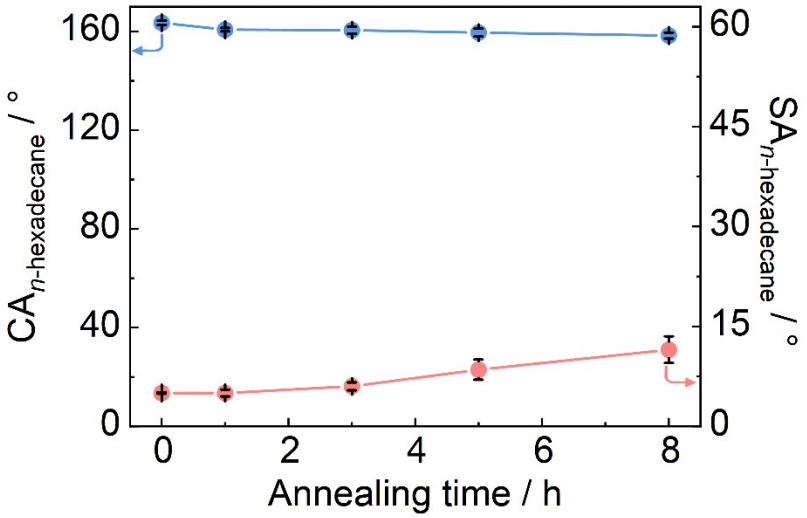

Fig. S5. Changes in $CA_{n\text{-hexadecane}}$ and $SA_{n\text{-hexadecane}}$ of the WPU/F-POS@SiO_2 coating with thermal aging time at 200 °C. Data are shown as mean ± SD, n = 5.

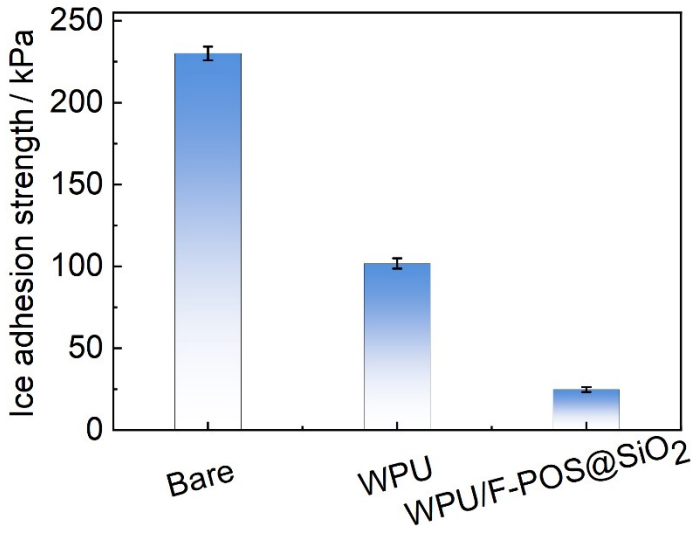

Fig. S6. Ice adhesion strength on bare Al plate, WPU coated Al plate and WPU/F-POS@SiO_2 coated Al plate in the -10 °C and 60% RH. Data are shown as mean ± SD, n = 3.

Table S1. Surface free energy of the WPU/F-POS@SiO_2 coatings prepared with different surfactants. Data are shown as mean ± SD, n = 3.

Surfactants	Surface free energy / mN/m
Free	11.6±0.05
FS-61	11.1±0.09
Zonyl 321	10.6±0.05
FS-3100	10.4±0.07

Table S2. CA and SA of the WPU/F-POS@SiO_2 coatings on various substrates. Data are shown as mean ± SD, n = 5.

Substrates	$CA_{n\text{-hexadecane}}$ / °	$SA_{n\text{-hexadecane}}$ / °
Glass	156.8±1.5	6.0±0.6
Magnesium alloy	162.8±2.5	7.8±0.5
Stainless steel	159.5±1.2	7.0±0.6
Aluminum alloy	169.2±2.5	5.0±0.9
Copper alloy	154.4±1.1	6.2±0.6